Noname manuscript No.
(will be inserted by the editor)

Formation of transverse cracks from the growth of multiple adjacent debonds on consecutive fibers in UD composites under transverse tension: Effect of the mutual position of debonds on Energy Release Rate

Luca Di Stasio · Janis Varna · Zoubir Ayadi

Received: date / Accepted: date

Abstract Models of Repeating Unit Cell (RUC) are developed to represent different Representative Volume Elements (RVEs) of UD composites of infinite size. Several damage states are studied in the form of different geometrical configurations of partially debonded and fully bonded fibers. It is found that the energetically most favorable cases for fiber/matrix interface crack (debond) growth are those where debonds grow on vertically (i.e. along thickness direction) aligned fibers. A maximum of Energy Release Rate (ERR) magnification is found when the vertically aligned partially debonded fibers are also contiguous.

Keywords Polymer-matrix Composites (PMCs) · Transverse Failure · Debonding · Finite Element Analysis (FEA)

1 Introduction

The process of damage onset and development in multi-axial Fiber Reinforced Polymer Composite (FRPC) laminates involves several fracture mechanisms, which concur to the final failure of the composite part. Upon loading, one of the first macroscopic mode of damage is the occurrence in transverse cracks in plies where fibers are not aligned with the remote applied loading. A single

Luca Di Stasio
Luleå University of Technology, University Campus, SE-97187 Luleå, Sweden
Université de Lorraine, EEIGM, IJL, 6 Rue Bastien Lepage, F-54010 Nancy, France
E-mail: luca.di.stasio@ltu.se

Janis Varna
Luleå University of Technology, University Campus, SE-97187 Luleå, Sweden
E-mail: janis.varna@ltu.se

Zoubir Ayadi
Université de Lorraine, EEIGM, IJL, 6 Rue Bastien Lepage, F-54010 Nancy, France
E-mail: zoubir.ayadi@univ-lorraine.fr

transverse crack does not significantly compromise the load-carrying of the laminate, but in large numbers transverse cracks become detrimental to the elastic response of the part under loading. Furthermore, high concentrantions of transverse cracks lead to stress re-distribution and stress concentrations that can promote other more dangerous mode of fracture, quickly leading to the global failure of the laminate or part. Understanding the factors that influence transverse cracks onset and propagation is thus fundamental to improve current laminate design and to identify mechanisms of controlled propagation, delay and suppression of transverse cracks. This would provide toughness to FRPC laminates and help to avoid early part replacement, and thus waste, currently in use to prevent sudden catastrophic brittle failure.

Early microscopic observations in glass fiber-epoxy cross-ply laminates determined that onset of transverse cracking occurs at the microscopic level in the form of fiber-matrix interface cracks (or debonds) [1]. Debonds grow along the arc direction of the fiber until reaching a critical size, then kink out of the interface and coalesce with other debonds across the ply thickness [20]. Once a through-the-thickness crack tunnels through the width of the laminate, a transverse crack is formed. Formation and growth of debonds at the microscale thus play a key role in the overall process of initiation of transverse cracking. To improve our understanding of the latter, the former must be studied and modeled.

The first investigations on the mechanics of fiber/matrix debonding proposed analytical models of a single partially debonded fiber placed in an infinite matrix. These models focused on understanding the effect of the elastic properties mismatch between fiber and matrix. They were firstly solved by Perlman and Sih [12], who provided the solution in terms of stress and displacement fields, and Toya [17], who evaluated the Energy Release Rate (ERR) at the debond tip. A closed-form analytical solution could only be found for the *open crack* case, which assumes that no contact between debond faces occurs. This solution was shown to provide, for large debonds, a non-physical solution that implies inter-penetration of crack faces [17,2]. Numerical treatment of the problem soon followed, in particular with the Boundary Element Method (BEM) solution by Paris et al. [10]. The numerical analysis of the single fiber model allowed first to understand the importance of crack face contact in the mechanics of fiber/matrix debonding [18], confirming earlier results regarding the straight bi-material interface crack [2]. The process of fiber/matrix debonding was investigated in models of a single partially debonded fiber embedded in an effectively infinite matrix under remote tension [10] and remote compression [3]. Residual thermal stresses were also analyzed [4]. The effect of a second nearby fiber was studied, under different uniaxial and biaxial tensile and compressive applied loads [5,6,14,15]. Debond growth in a hexagonal cluster of fibers embedded in an effectively homogenized UD composite was investigated by Zhuang et al. [21]. The interaction of two debonds facing each other on two nearby fibers was addressed in [19] for a cluster of fibers immersed in a homogenized UD.

Models of kinking were developed for a single fiber in an infinite matrix [11]

and a partially debonded fiber in a cluster of fibers inside a homogenized UD [22]. A study on linking of debonds was proposed in [19].
An analysis of the configuration preceding kinking and linking thus seems to lacking in the literature. We devote our attention in this paper to the analysis of Representative Volume Elements (RVEs) which model the presence of muliple debonds on fibers aligned across the thickness of UD composites. We focus on understanding the effect of the mutual interaction of consecutive debonds in the vertical direction and of their relative position, i.e. on the same or opposite sides of their respective fibers. We are interested in identifying which mechanisms might favor debond growth and which might, on the other hand, prevent it. For this reason, we select a regular arrangement of fibers and we adopt the approach of Linear Elastic Fracture Mechanics (LEFM) to characterize debond growth, by evaluating Mode I and Mode II Energy Release Rate (ERR). The Finite Element Method (FEM) is chosen to compute stress, strain and displacement fields, which are required to estimate ERR. The characteristics of the RVEs and the Finite Element (FE) solution are described in Sec. 2; the main results are reported and discussed in Sec. 3 and the main conclusions presented in Sec. 4.

2 RVE models & FE discretization

2.1 Introduction, properties and nomenclature

We focus in this article on debond growth in unidirectional (UD) composites subjected to in-plane transverse tensile loading. In particular, the interaction between debonds is studied through the development of models of Representative Volume Elements (RVE) of laminates with different configurations of debonds (see Fig. 1 and Fig. 2).

In order to facilitate the description of the models, let us assume that the UD composite mid-plane lies in the $x-y$ plane, where y coincides with the UD $0°$ direction while the $x-axis$ represents the UD in-plane transverse direction. Axis z is the through-the-thickness direction of the composite.

The composite RVE is defined in the $x-z$ plane and is repeating both along x and z. Mathematically, it corresponds to an infinite UD composite which models, practically, the behavior of debonds located far away from the laminate free surfaces. i.e. close to the laminate mid-plane, in a relatively thick UD composite (thickness $>$ 100 fiber diameters). The composite with debonds is modeled as a sequence of fiber rows with or without debonds stacked on each other in the vertical (through-the-thickness) direction. Notice that each row contains only one fiber in the vertical direction. A regular microstructure is adopted for all RVEs, with fibers organized in a square-packing configuration. This choice is motivated by our interest in investigating the mechanisms that favors or prevent debond growth, and not in simulating crack path evolution in an arbitrary, randomized distribution of fibers. The regularity of the square-packing arrangement allows the identification of the different mecha-

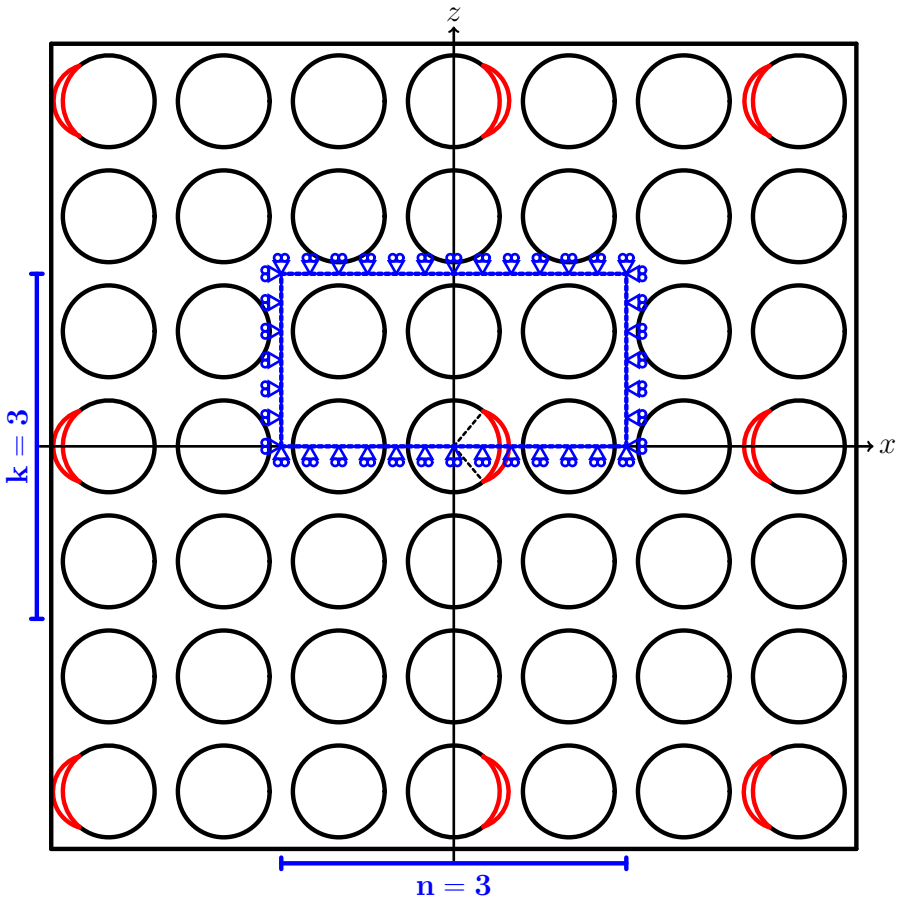

Fig. 1: Representative Volume Element $n \times k - symm$ of a UD composite with debonds appearing after $n-1$ and after $k-1$ undamaged fibers respectively in the horizontal and vertical direction. In the vertical direction, on fibers belonging to the same "column", debonds are located always on the same side.

nisms influencing debond growth. Given their square-packing arrangement of fibers, each RVE is built by using the unit cell in Figure 3 as the basic building block. The unit cell contains one fiber place in its center and has a size of $2L \times 2L$, where

$$L = \frac{R_f}{2}\sqrt{\frac{\pi}{V_f}}. \tag{1}$$

In Equation 1, V_f is the fiber volume fraction and R_f the fiber radius. The fiber volume fraction is assumed equal to 60% in each RVE and the fiber radius equal to $1\mu m$. The choice of the previous value is not dictated

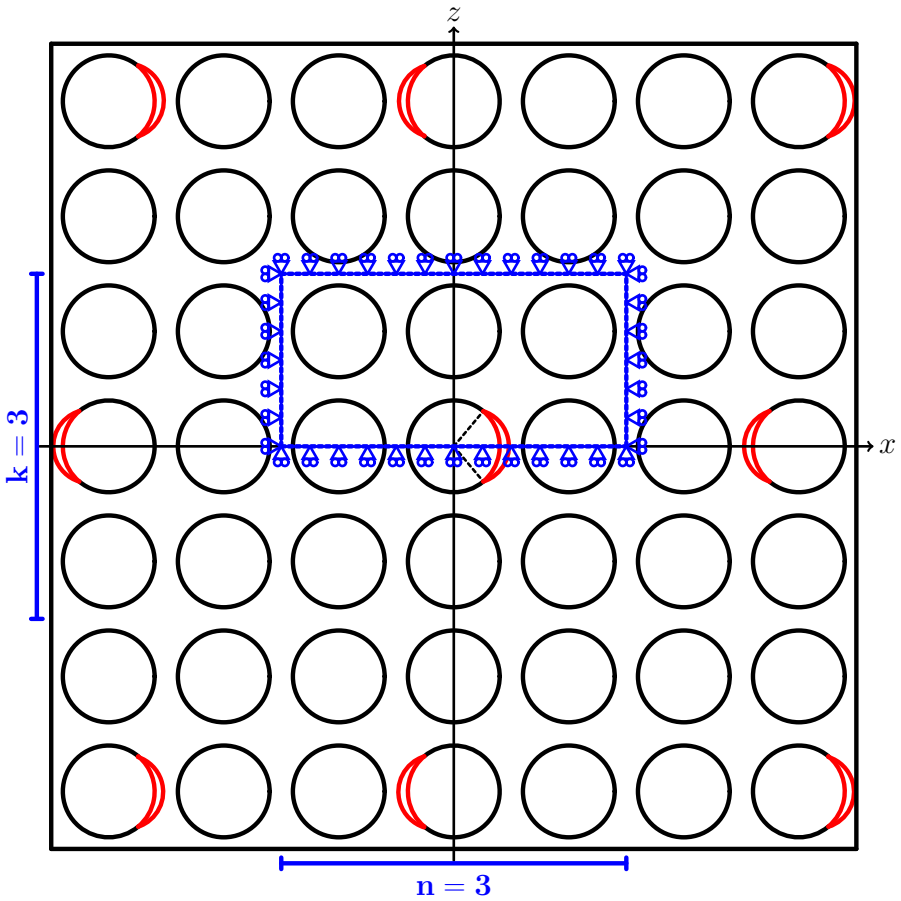

Fig. 2: Representative Volume Element $n \times k - asymm$ of a UD composite with debonds appearing after $n-1$ and after $k-1$ undamaged fibers respectively in the horizontal and vertical direction. In the vertical direction, on fibers belonging to the same "column", debonds are located on the opposite sides of consecutive fibers.

by physical considerations but by simplicity. It is thus useful to remark here that, in a linear elastic solution as the one considered in the present work, the ERR is proportional to the geometrical dimensions of the model and, consequently, recalculation of the ERR for fibers of any size requires a simple multiplication. Notice also that, given the relationship in Eq. 1 and that the unit cell is identically repeated following a square-packing configuration, V_f is homogeneous, i.e. no clustering of fibers is considered.

A glass fiber-epoxy UD composite is treated in the present work, and it is assumed that the response of each phase lies always in the linear elastic domain. The material properties of glass fiber and epoxy are reported in Table 1.

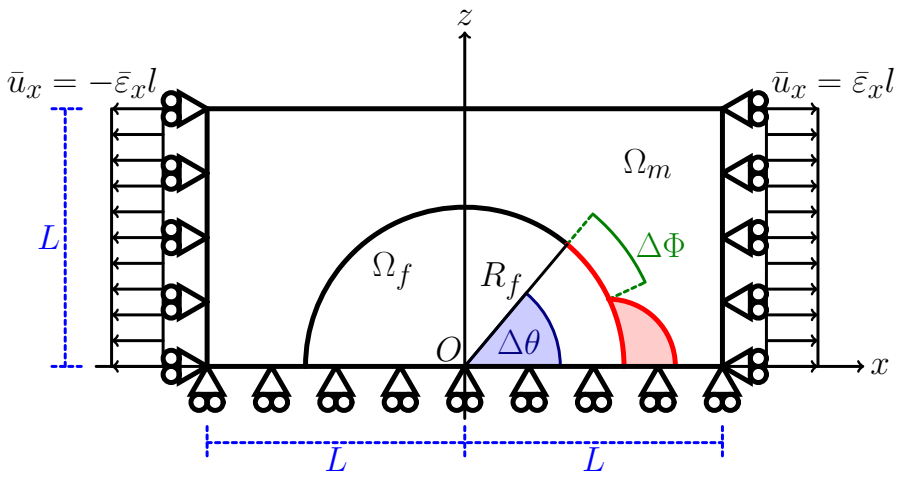

Fig. 3: Schematic of the model with its main parameters.

Table 1: Summary of the mechanical properties of fiber and matrix. E stands for Young's modulus, μ for shear modulus and ν for Poisson's ratio.

Material	$E\,[GPa]$	$\mu\,[GPa]$	$\nu\,[-]$
Glass fiber	70.0	29.2	0.2
Epoxy	3.5	1.25	0.4

We consider that upon application of a load in the x-direction, the strain response in the y-direction is small due to the very small minor Poisson's ratio of the UD composite. We also assume that debond size to be significantly larger in the fiber longitudinal direction than in the arc direction. We therefore use 2D models under the assumption of plane strain defined in the $x-z$ section of the composite, which allows us to focus our interest on debond growth along the arc direction. Assumptions of generalized plane strain would be more suited to represent the physics, however it would limit the scope of comparisons with previous studies in the literature. It is for this reason that plane strain conditions are preferred.
All RVEs are symmetric with respect to the horizontal direction, thus only half of the RVE is explicitly modeled and symmetry conditions are applied to the lower boundary of the RVE (Fig. 1 and Fig. 2). The number n of fibers in the horizontal directions and k in the vertical direction belonging to the RVEdetermine the total size of the RVE, described by its total length l and total height h:

$$l = n2L \qquad h = k2L; \tag{2}$$

where $2L$ is the side length of the square unit cell previously introduced and L is defined according to Eq. 1. The number of fibers in the horizontal and vertical directions determine as well the damage state of the modeled UD

composite. In particular, a $n \times k$ RVE represents a UD composite in which a debond appear after $n-1$ fully bonded fibers inside a fiber row, and a fiber row contains debonds after $k-1$ fiber rows with no damage (see Fig. 1 and Fig. 2). To model such configurations, conditions of coupling of the horizontal displacement u_x are applied to the right and left boundary, which ensures that the computed solution represents a model in which the RVE is repeated infinite times in the horizontal direction. It is worth to highlight that the repetition of the RVE occurs in a mirror-like fashion: moving along the x-axis, if a debond appears on the right side of its fiber, the next one is placed on the left side.
This might lead to extreme conditions in the model. Consider for example the case of $1 \times k$ RVEs: inside a fiber row containing damage, an infinite number of debonds is present and debonds are facing each other pair-by-pair. Such configuration is physically unlikely, however the evaluation of the ERR in this case provides a bound for the case of maximum debond mutual interaction in the vertical direction. Thus, the models proposed here might represent extreme configuration, but they provide theoretical bounds for debond behavior in an actual composite. In particular, observations regarding mechanisms favoring debond growth will represent an upper bound on ERR and thus a conservative estimation of the actual behavior, still of use for the structural designer. Greater care should instead be taken when considering mechanisms preventing debond growth: the ERR estimate provided by our models would be a lower bound, thus debond growth might be higher than predicted in the actual composite.
Repetition occurs also along the vertical direction. Here two cases can be distinguished: first, debonds aligned in the vertical direction are placed on the same side of their respective fibers as in Figure 1; second; debonds aligned in the vertical direction are placed on alternating opposite sides of their respective fibers in Figure 2. The first is case of symmetric repetition with respect to the upper boundary of the RVE; the second case is one of anti-symmetric repetition with respect to the upper boundary of the RVE. The two different families of RVEs (symmetric with respect to anti-symmetric repetition) are thus respectively called $n \times k - symm$ and $n \times k - asymm$. The details of the boundary conditions adopted in the two different cases are described in Sec. 2.2.

2.2 Equivalent boundary conditions: description and validation

Two main families of Representative Volume Elements have been introduced in the previous section, distinguished by their pattern of repetition along the vertial direction: $n \times k - symm$ and $n \times k - asymm$.
To model the symmetric repetition of $n \times k - symm$ RVE (Fig. 1) we adopt,

on the upper boundary, conditions of coupling of the vertical displacements u_z of the type

$$u_z(x,h) = \bar{u}_z, \tag{3}$$

where h is the total height of the RVE defined in Eq. 2 and $\bar{u}_z$ is the constant value of the vertical displacement, equal for all the points on the upper boundary. The value of $\bar{u}_z$ is *a priori* unknown and is evaluated as part of the elastic solution.
The asymmetric repetition of $n \times k - asymm$ RVE (Fig. 2) is modeled with the following set of conditions applied to the vertical u_z and horizontal displacements u_x:

$$\begin{aligned} u_z(x,h) - u_z(0,h) &= -\left(u_z(-x,h) - u_z(0,h)\right) \\ u_x(x,h) &= -u_x(-x,h), \end{aligned} \tag{4}$$

where h is again the total height of the RVE and $u_z(0,h)$ is the vertical displacement of the upper boundary mid-point, which is always located at coordinates $(0,h)$. Similarly to $\bar{u}_z$ in the symmetric case, $u_z(0,h)$ is *a priori* unknown and is computed as part of the elastic solution.

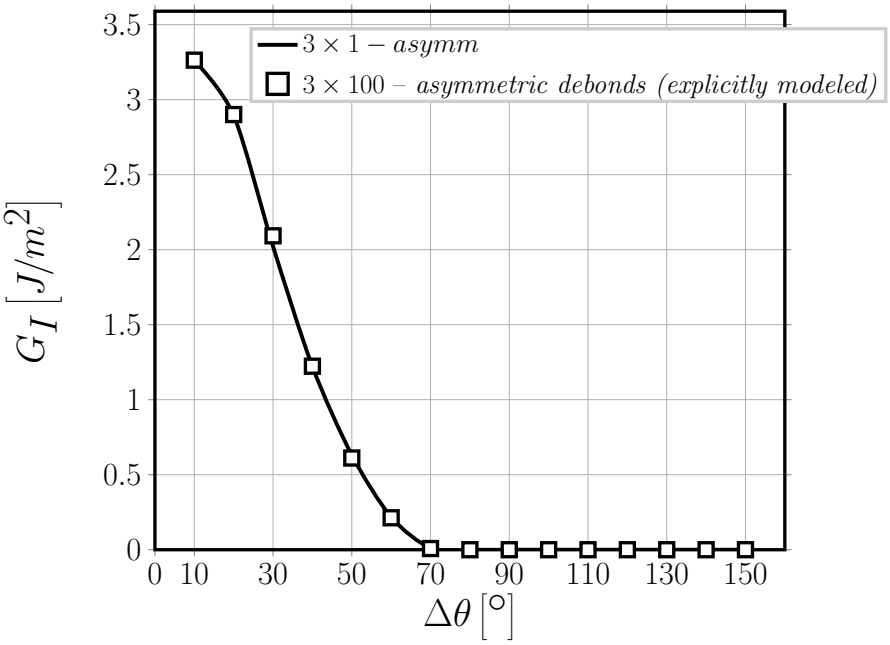

Fig. 4: Validation of asymmetric coupling conditions of Eq. 4: Mode I ERR, $V_f = 60\%$, $\bar{\varepsilon}_x = 1\%$.

To the authors' knowledge, this is the first time the set of boundary conditions of Eq. 4 is proposed and used to model an asymmetric coupling as the one reported in Figure 2. To validate them, Mode I (Fig. 4) and Mode II ERR (Fig. 5) are evaluated for $3\times1-asymm$ RVE and compared with the results of the $3\times100-asymmetric\ debonds$ (*explicitly modeled*) RVE, in the case of an applied strain $\bar{\varepsilon}_x$ of 1%. The $3\times201-asymmetric\ debonds$ (*explicitly modeled*) RVE possesses, as all other RVEs studied here, conditions of coupling of the horizontal displacement applied to the left and right side. It is as well symmetric with respect to the x-axis, thus only half of the RVE is modeled and conditions of symmetry are applied to the lower horizontal boundary. The upper side of the RVE is, differently from the other models studied here, left free. Debonds are explicitly modeled and placed on alternating sides of vertically aligned fibers, i.e. if a fiber has a debond on the right side the next fiber above will have the debond on the left side. Debonds are all of the same size. The $3\times201-asymmetric\ debonds$ (*explicitly modeled*) RVE thus represents the same configuration as the $3\times1-asymm$ RVE, but explicitly modeled. Comparison of the ERR of the two RVEs provides a validation of accuracy of the conditions expressed in Eq. 4 as a mean to represent the situation with alternating debonds (or asymmetric coupling, as depicted in Fig. 2 with the use of equivalent boundary conditions, which is a more effective in terms of computational cost of the model (time and memory needed to compute the solution).

As shown in Figure 4 and Figure 5, a very good agreement is obtained between the results of the two RVEs for both Mode I and Mode II ERR. The validity of the asymmetric coupling conditions proposed in Equation 4 is thus confirmed.

2.3 Finite Element (FE) solution

The solution of the elastic problem is obtained with the Finite Element Method (FEM) within the Abaqus environment, a commercial FEM software [16].
The debond is placed symmetrically with respect to the x axis (see Fig. 3) and it is characterized by an angular size of $\Delta\theta$ (making the full debond size equal to $2\Delta\theta$). For large debond sizes (at least $\geq 60^\circ - 80^\circ$), a region $\Delta\Phi$ of variable size appears at the crack tip where the crack faces are in contact but free to slide relatively to each other. In order to model crack faces motion in the contact zone, frictionless contact is considered between the two crack faces to allow free sliding and avoid interpenetration.
Meshing of the model is accomplished with second order, 2D, plane strain triangular (CPE6) and quadrilateral (CPE8) elements. A regular mesh of 8-node (2^{nd} order rectangular) elements with almost unitary aspect ratio is enforced at the crack tip in order to ensure the convergence of the ERR. The angular size δ of an element in the crack tip neighborhood is always equal to 0.05°. The crack faces are modeled as element-based surfaces and a small-sliding contact pair interaction with no friction is imposed between them.

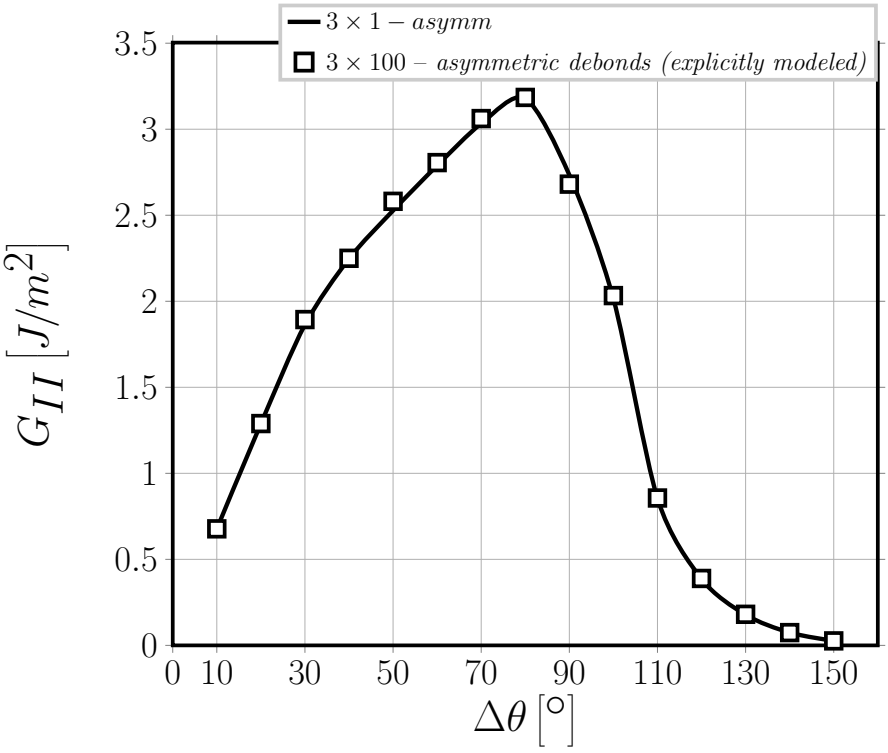

Fig. 5: Validation of asymmetric coupling conditions of Eq. 4: Mode II ERR, $V_f = 60\%$, $\bar{\varepsilon}_x = 1\%$.

The Mode I, Mode II and total Energy Release Rates (ERRs) (respectively referred to as G_I, G_{II} and G_{TOT}) are the main result of FEM simulations; they are evaluated using the VCCT [9] implemented in a in-house Python routine. Validation is performed with respect to the results reported in [11, 14], which were obtained with the Boundary Element Method (BEM) for a model of a partially debonded single fiber placed in an infinite matrix. As discussed in more detail in [8], the agreement between FEM (present work) and BEM [11,14] solutions is good and the difference between the two does not exceed 5%. This provides us with a level of uncertainty with which we can analyze the significance of observed trends: any relative difference in ERR between different RVEs smaller than 5% cannot be reliably distinguished from numerical uncertainty and its discussion should thus be avoided.

3 Results & Discussion

3.1 Interaction between isolated debonds in infinite UD composites

The effect on Mode I and Mode II ERR of the interaction between debonds appearing at regular distances (in terms of fully bonded fibers) in the horizontal and vertical directions (models $n \times k - coupling$) is shown respectively in Figure 6 and Figure 7. It can be observed that it is the distance between debonds in the horizontal direction that presents a relevant effect on ERR: the number of fully bonded fibers between consecutive debonds in the vertical direction has a negligible influence on Mode I and a very modest effect, below or at the limit of the 5% accuracy of the model, on Mode II.

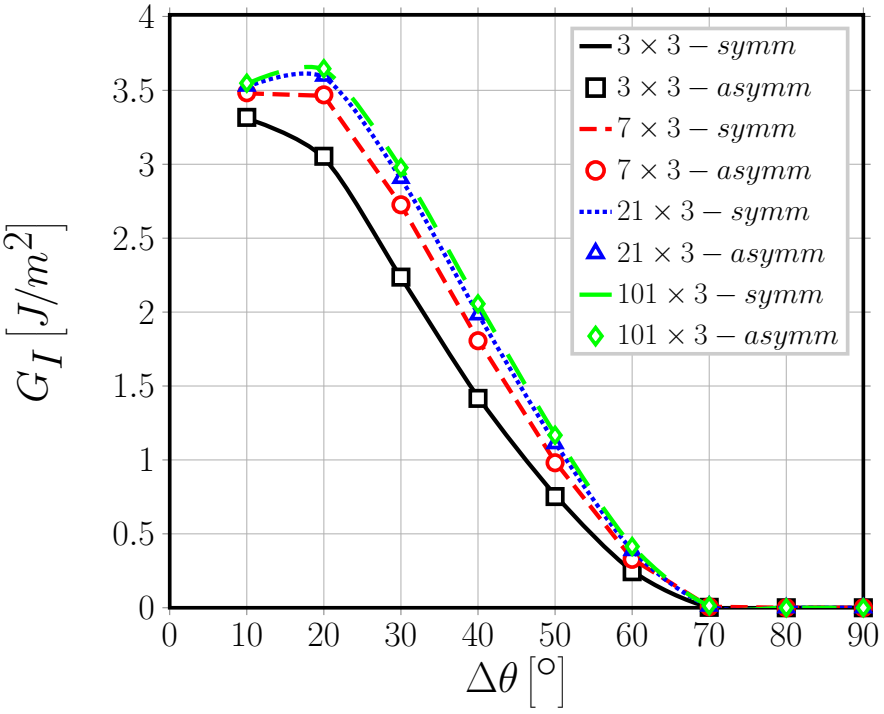

Fig. 6: Effect of debond-debond interaction in infinite UD composites on Mode I ERR: models $n \times k - coupling$. $V_f = 60\%$, $\varepsilon_x = 1\%$.

On the other hand, increasing the number of fully bonded fibers between debonds in the horizontal direction leads to a significant increase in both Mode I and Mode II ERR, due to the magnification of the x-strain in the crack tip neighborhood [8]. A critical distance (in terms of undamaged fibers) at which a non-interacting solution can be observed is apparent for Mode I (Figure 6). Given that Mode II ERR for models $21 \times 3 - coupling$, $21 \times 21 - coupling$,

$101 \times 3 - coupling$ and $101 \times 101 - coupling$ is in a $\leq 5\%$ range with respect to each other and thus their difference is not significant taking into account model accuracy, it can be argued that also in Mode II a critical distance exists at which a non-interacting solution appears.

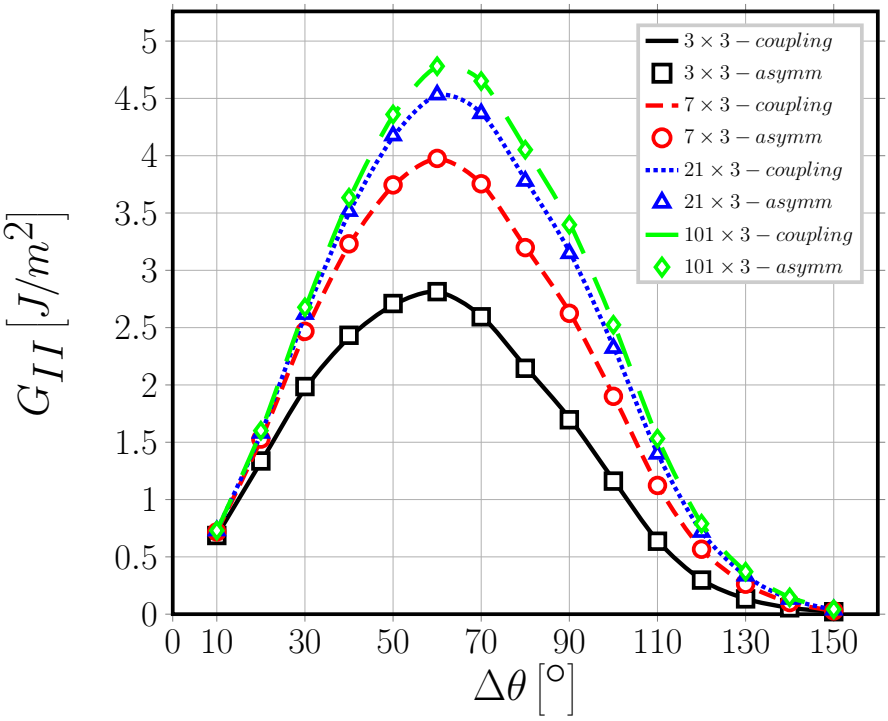

Fig. 7: Effect of debond-debond interaction in infinite UD composites on Mode II ERR: models $n \times k - coupling$. $V_f = 60\%$, $\varepsilon_x = 1\%$.

3.2 Debond-debond interaction between horizontal rows of partially debonded fibers in infinite UD composites

The results presented in Figures 8 and 9 for respectively Mode I and Mode II ERR of models $1 \times k - coupling$ confirm the observations presented in Section 3.1. Models $1 \times k - coupling$ represents the RVE of an infinite UD composite with horizontal fiber rows that appear at regular intervals (measured in terms of fully bonded fibers) and in which fibers are all partially debonded (see Fig. **??** for reference).

Varying the number k of undamaged fibers between fiber rows of only partially debonded fibers does not have any effect on ERR, neither in Mode I (Figure 8) nor in Mode II (Figure 9). The observations of Sec. 3.1 are thus

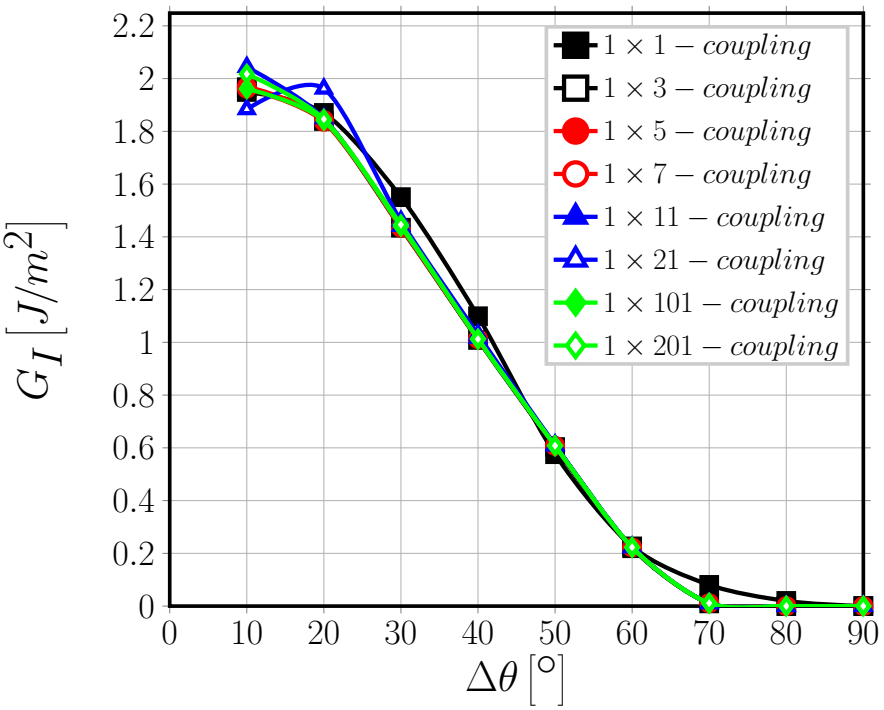

Fig. 8: Effect of debond-debond interaction in infinite UD composites on Mode I ERR: models $1 \times k - coupling$. $V_f = 60\%$, $\varepsilon_x = 1\%$.

confirmed: it is the presence of fully bonded fibers only in the horizontal direction, i.e. the loading direction, that affects the debond ERR through x-strain magnification.

3.3 Debond-debond interaction between vertical lines of partially debonded fibers in infinite UD composites

Figures 10 and 11 report respectively Mode I and Mode II ERR for models $1 \times k - coupling$, which correspond to the RVEs of UD composites with vertical lines of partially debonded fibers appearing at regular intervals (in terms of undamaged fibers) in the horizontal direction (see Fig. 2 for reference).

As it can be expected from the discussion of Sec. 3.1 and Sec. 3.2, increasing the number of fully bonded fibers between two consecutive lines of partially debonded fibers is responsible for significant increases in both Mode I and Mode II ERR.

However, comparison of Fig. 10 with Fig. 8 and of Fig. 11 with Fig. 9 provides an additional interesting result: the presence of fully bonded fibers between debonds appearing on vertically aligned fibers reduces both G_I and

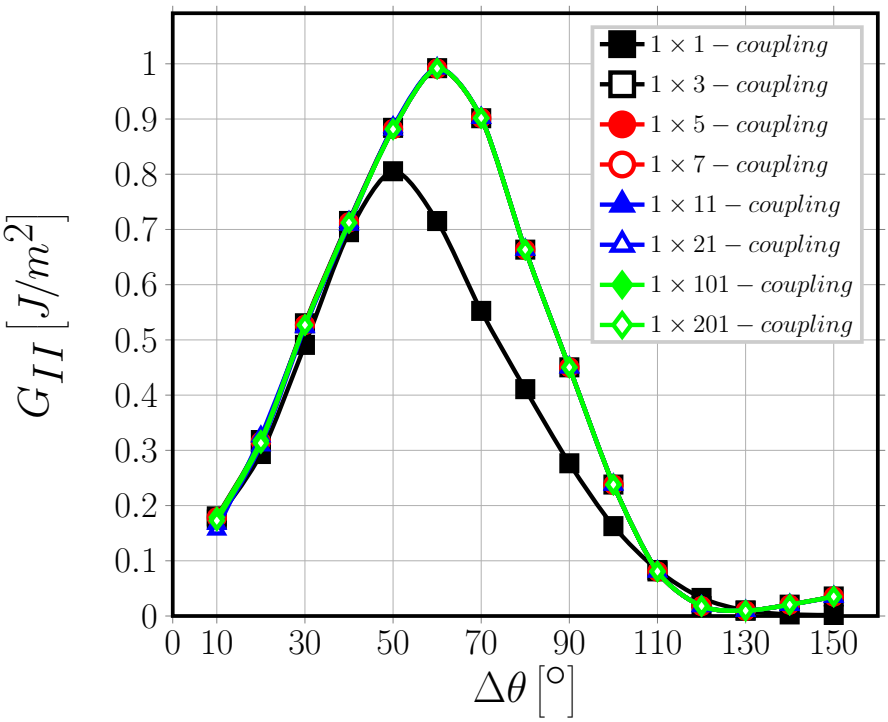

Fig. 9: Effect of debond-debond interaction in infinite UD composites on Mode II ERR: models $1 \times k - coupling$. $V_f = 60\%$, $\varepsilon_x = 1\%$.

G_{II}. On the other hand, for the same horizontal distance between debonded fibers, the energetically most favorable configuration is achieved when debonds are contiguous along the vertical direction. Two further effects can be observed: the onset of the contact zone is delayed up to a debond size of $\sim 100°$ (Fig. 10); the peak value of G_{II} is shifted to a debond size of up to $90°$ (Fig. 11). Thus, larger debonds are in general favored. This behavior can be related to the local deformation of the matrix. Between two vertically aligned debonds, the matrix strip between the two partially debonded fibers has, locally, both the lower and the upper surface free to deform. Due to Poisson's effect, the two surfaces move towards each other, imposing an opening displacement on the crack tip. This in turn favors Mode I and delays the onset of the contact zone. Furthermore, taking into account that fibers are more rigid than the sorrounding matrix, when the fiber on top of the debonded one is undamaged (fully bonded), the x-displacement field in the matrix is restrained by the requirement of continuity at the interface. When instead another partially debonded fiber is present, a matrix strip is created with an upper and lower free surfaces, i.e. detached from the upper and lower fibers. The displacement field in this matrix strip is thus not restrained by the more rigid fibers and a magnification effect of the $x - strain$ takes place. This in turn causes an increase in G_I for smaller

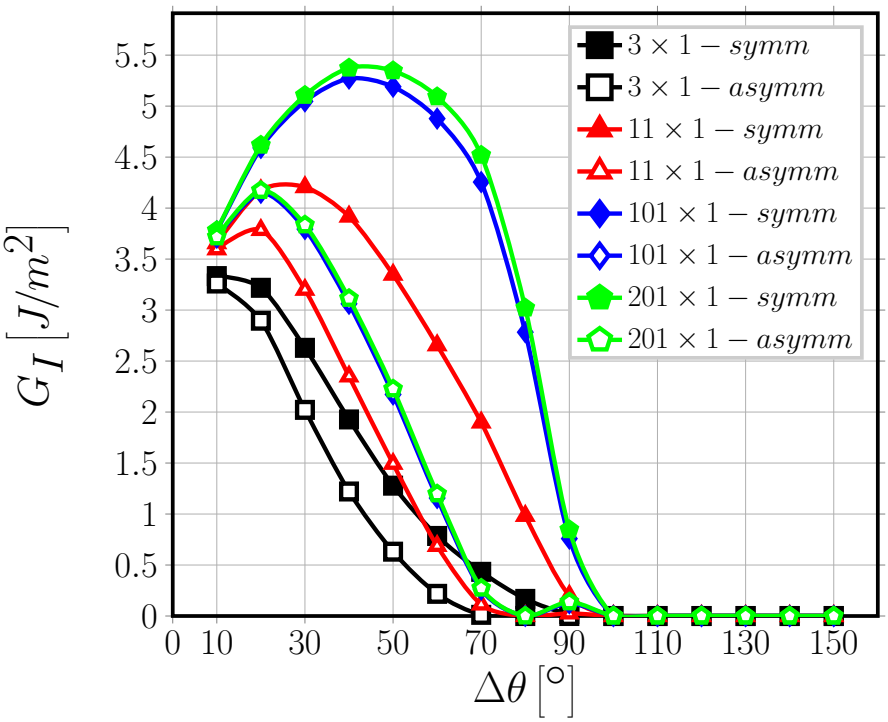

Fig. 10: Effect of debond-debond interaction in infinite UD composites on Mode I ERR: models $n \times 1 - coupling$. $V_f = 60\%$, $\varepsilon_x = 1\%$.

debonds (the x-displacement is the major component of the crack opening displacement at the crack tip) and in G_{II} for larger ones (the x-displacement is the major component of the crack shear displacement at the crack tip).

4 Conclusions

Different models of infinite UD composites have been studied with different configurations of multiple interacting debonds in order to investigate their effect of Mode I and Mode II Energy Release Rate.
Building upon the observations made in the previous section, several conclusions can be drawn about the growth of debonds in UD composites:

- at given strain level, multiple debonds can appear on not consecutive vertically-aligned fibers;
- at a given strain level, the vertical lines of fibers on which debonds grow are determined by the horizontal distance from pre-existing debonds;
- a minimum non-interactive distance exists for the Energy Release Rate;
- when spacing between vertical lines of debonds is lower than the minimum non-interactive distance, the ERR decreases;

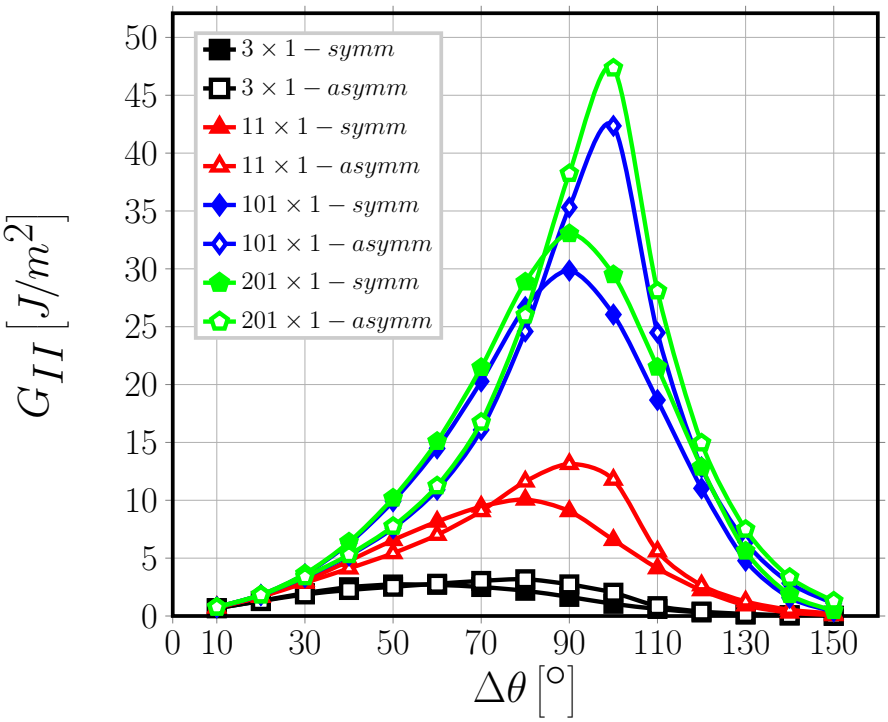

Fig. 11: Effect of debond-debond interaction in infinite UD composites on Mode II ERR: models $n \times 1 - coupling$. $V_f = 60\%$, $\varepsilon_x = 1\%$.

– thus, conversely, when spacing between vertical lines of debonds is lower than the minimum non-interactive distance, higher levels of strain are needed to grow debonds;
– growth of debonds appearing on contiguous vertically-aligned fibers is energetically the most favorable;
– larger debonds are favored on contiguous vertically aligned partially debonded fibers.

Acknowledgements Luca Di Stasio gratefully acknowledges the support of the European School of Materials (EUSMAT) through the DocMASE Doctoral Programme and the European Commission through the Erasmus Mundus Programme.

References

1. Bailey, J.E., Parvizi, A.: On fibre debonding effects and the mechanism of transverse-ply failure in cross-ply laminates of glass fibre/thermoset composites. Journal of Materials Science **16**(3), 649–659 (1981). DOI 10.1007/bf02402782
2. Comninou, M.: The interface crack. Journal of Applied Mechanics **44**(4), 631 (1977). DOI 10.1115/1.3424148

3. Correa, E., Gamstedt, E., París, F., Mantič, V.: Effects of the presence of compression in transverse cyclic loading on fibre–matrix debonding in unidirectional composite plies. Composites Part A: Applied Science and Manufacturing **38**(11), 2260–2269 (2007). DOI 10.1016/j.compositesa.2006.11.002
4. Correa, E., Mantič, V., París, F.: Effect of thermal residual stresses on matrix failure under transverse tension at micromechanical level: A numerical and experimental analysis. Composites Science and Technology **71**(5), 622–629 (2011). DOI 10.1016/j.compscitech.2010.12.027
5. Correa, E., París, F., Mantič, V.: Effect of the presence of a secondary transverse load on the inter-fibre failure under tension. Engineering Fracture Mechanics **103**, 174–189 (2013). DOI 10.1016/j.engfracmech.2013.02.026
6. Correa, E., París, F., Mantič, V.: Effect of a secondary transverse load on the inter-fibre failure under compression. Composites Part B: Engineering **65**, 57–68 (2014). DOI 10.1016/j.compositesb.2014.01.005
7. Correa, E., Valverde, M.I., Velasco, M.L., París, F.: Microscopical observations of inter-fibre failure under tension. Composites Science and Technology **155**, 213–220 (2018). DOI 10.1016/j.compscitech.2017.12.009
8. Di Stasio, L., Varna, J., Ayadi, Z.: Energy release rate of the fiber/matrix interface crack in UD composites under transverse loading: effect of the fiber volume fraction and of the distance to the free surface and to non-adjacent debonds. Theoretical and Applied Fracture Mechanics p. 102251 (2019). DOI 10.1016/j.tafmec.2019.102251
9. Krueger, R.: Virtual crack closure technique: History, approach, and applications. Applied Mechanics Reviews **57**(2), 109 (2004). DOI 10.1115/1.1595677
10. París, F., Caño, J.C., Varna, J.: The fiber-matrix interface crack — a numerical analysis using boundary elements. International Journal of Fracture **82**(1), 11–29 (1996). DOI 10.1007/bf00017861
11. París, F., Correa, E., Mantič, V.: Kinking of transversal interface cracks between fiber and matrix. Journal of Applied Mechanics **74**(4), 703 (2007). DOI 10.1115/1.2711220
12. Perlman, A., Sih, G.: Elastostatic problems of curvilinear cracks in bonded dissimilar materials. International Journal of Engineering Science **5**(11), 845–867 (1967). DOI 10.1016/0020-7225(67)90009-2
13. Rice, J.R.: A path independent integral and the approximate analysis of strain concentration by notches and cracks. Journal of Applied Mechanics **35**(2), 379 (1968). DOI 10.1115/1.3601206
14. Sandino, C., Correa, E., París, F.: Numerical analysis of the influence of a nearby fibre on the interface crack growth in composites under transverse tensile load. Engineering Fracture Mechanics **168**, 58–75 (2016). DOI 10.1016/j.engfracmech.2016.01.022
15. Sandino, C., Correa, E., París, F.: Interface crack growth under transverse compression: nearby fibre effect. In: Proceeding of the 18^{th} European Conference on Composite Materials (ECCM-18) (2018)
16. Simulia, Providence, RI, USA: ABAQUS/Standard User's Manual, Version 6.12 (2012)
17. Toya, M.: A crack along the interface of a circular inclusion embedded in an infinite solid. Journal of the Mechanics and Physics of Solids **22**(5), 325–348 (1974). DOI 10.1016/0022-5096(74)90002-7
18. Varna, J., París, F., C.Caño, J.: The effect of crack-face contact on fiber/matrix debonding in transverse tensile loading. Composites Science and Technology **57**(5), 523–532 (1997). DOI 10.1016/s0266-3538(96)00175-3
19. Varna, J., Zhuang, L.Q., Pupurs, A., Ayadi, Z.: Growth and interaction of debonds in local clusters of fibers in unidirectional composites during transverse loading. Key Engineering Materials **754**, 63–66 (2017). DOI 10.4028/www.scientific.net/kem.754.63
20. Zhang, H., Ericson, M., Varna, J., Berglund, L.: Transverse single-fibre test for interfacial debonding in composites: 1. experimental observations. Composites Part A: Applied Science and Manufacturing **28**(4), 309–315 (1997). DOI 10.1016/s1359-835x(96)00123-6
21. Zhuang, L., Pupurs, A., Varna, J., Talreja, R., Ayadi, Z.: Effects of inter-fiber spacing on fiber-matrix debond crack growth in unidirectional composites under transverse loading. Composites Part A: Applied Science and Manufacturing **109**, 463–471 (2018). DOI 10.1016/j.compositesa.2018.03.031

22. Zhuang, L., Talreja, R., Varna, J.: Transverse crack formation in unidirectional composites by linking of fibre/matrix debond cracks. Composites Part A: Applied Science and Manufacturing **107**, 294–303 (2018). DOI 10.1016/j.compositesa.2018.01.013